Proceedings of the ASME 2019 6th International Conference
on Micro/Nanoscale Heat and Mass Transfer
MNHMT2019
July 8-10, 2019, Dalian, China

MNHMT2019-4181

FLUID MIXING USING INDUCED CHARGE ELECTRO-OSMOTIC TRANSVERSE FLOW ACTUATED BY ASYMMETRICAL DRIVING ELECTRODE SEQUENCE

Xiaoming Chen[1], Yukun Ren[*1,2,3], Likai Hou[1], Tianyi Jiang[1], and Hongyuan Jiang[*1,2]

[1]School of Mechatronics Engineering, Harbin Institute of Technology, Harbin, China
[2]State Key Laboratory of Robotics and System, Harbin Institute of Technology, Harbin, China
[3]State Key Laboratory of Nonlinear Mechanics, Chinese Academy of Sciences, Beijing, China

ABSTRACT

Microfluid mixing is an essential process in chemical analysis, drug test, and nanoparticle synthesis. Induced charge electro-osmosis (ICEO) has good capability in microfluid mixing for its reconfigurable vortex profile. We found experimentally ICEO transverse flow induced by the asymmetrical driving electrode has a good performance in disturbing the interface of two fluids. Encouraged by these aspects, we proposed a micromixer using ICEO transverse flows actuated by the asymmetrical driving electrode sequence to mix microfluids. We established a simulation model to investigate the evolution of the interface and demonstrate the work principle of this method. Moreover, we numerically explored the effects of device structure, and electrolyte characteristics on the capability of micromixer. Finally, we validated this method experimentally, and studied the effects of voltage intensity, frequency and flow rate on the mixing capability, obtaining mixing efficiency exceeding 94%. This method is a potential alternative in various microfluidic and lab-on-a-chip applications.

Keywords: Microfluid mixing, Induced charge electro-osmosis, Transverse flow, Asymmetrical driving electrode sequence, Lab on a chip.

1 INTRODUCTION

Fluid mixing in microfluidic device is an essential process in many chemical applications [1-3], such as chemical analysis [4], drug test, and nanoparticle synthesis [5-7]. In response to this situation, ongoing literatures have been published to report microfluidic devices for efficient and effective fluid mixing. The devices for microfluid mixing can be classified into two broad categories, passive and active [8-10]. Passive micromixers in general contain baffles or obstacles to stretch the interface of fluids, which may involve the complicated fabrication of microchannel [5, 11-13]. Moreover, non-ignorable sample dilution will occur in the passive micromixers, which contributes to a loss of assay sensitivity [9,10].

Active micromixers don't subject to these problems [10]. Importantly, active devices can be controlled flexibly by adjusting the external fields. In recent years, many active micromixers have been developed based on various mechanisms, including acoustical wave [14], magnetic force, temperature field [15], and electric field [2,16]. Although acoustical micromixer is non-invasive and flexible in mixing microfluids, this device requires expensive acoustical-wave generator and complicated fabrication [14]. The micromixers based on magnetic force have excellent performance, whereas these devices have special requirement for the liquid samples [17] or need magnetic stir part [18]. Despite temperature-programmed micromixer has important application in biochemical reaction, this method may be vulnerable to environment temperature change [15]. Compared to these active micromixers mentioned above, micromixers based on electric field have many advantages, such as simple structure, ease of

---
* Yukun Ren: rykhit@hit.edu.cn; Hongyuan Jiang: jhy_hit@hit.edu.cn.
  School of Mechatronics Engineering and State Key Laboratory of Robotics and System, Harbin Institutfe of Technology, Harbin, China;

integration and easy operation [19]. Moreover, numerous micromixers based on electrokinetics, involving AC electro-osmosis (ACEO) [20], AC electro-thermal (ACET) [16, 21] and induced charge electro-osmosis (ICEO) [22, 23], have been developed to achieve microfluid mixing.

Recently, among the electrokinetically driven mixing devices, ICEO-vortex-based micromixers have received considerable attention for its good performance in controlling the fluid [24, 25]. For this merit of ICEO vortices, many microfluidic devices have been developed to manipulate the particle samples. Ren et al took advantage of symmetrical ICEO vortices to concentrate the particle samples [26-28]. Liu et al developed a sample concenter and director by applied the AC-flow field effect transistor (AC-FFET) into ICEO vortices [29]. Chen et al made use of ICEO focusing characterization to deal with the issue that dielectrophoresis (DEP)-force based separation rely on hydrodynamic focusing, which requires an encumbering peripheral system and a complicated operation to drive and control the fluid motion [30]. Wu et al proposed a microfluidic device for single cell trapping, which provides a useful tool for cell analysis [31]. It is worth noting that these devices are developed by controlling ICEO vortex profile to indirectly manipulate the particle samples. More interestingly, ICEO vortices can be reconfigured by adjusting the distribution of external electric field, and structure of floating or driving electrodes, which coincidentally meets the requirement of breaking fluid interface [8]. Therefore, ICEO flow has a great potential in disturbing the interface of fluids and developing micromixer.

Since Bazant and Squires proposed ICEO flow [32], many literatures about ICEO-based microfluid mixing were reported [33,34]. Qian et al in 2002 theoretically studied the electro-osmotic flows in a conduit with nonuniform zeta potentials along its walls, and asserted that their proposed electro-osmotic stirrers may be particularly beneficial for microfluidic mixers [35]. Successively, Zhao et al in 2007 also proposed a microfluidic chaotic stirrer utilizing ICEO, which consists of a concentric annulus whose outer surface is defined by an array of electrodes that provide a spatially varying potential distribution [36]. Then, many novel ICEO-based micromixers have been put forward and validated experimentally. Cindy Harnett et al in 2008 developed a micromixer and characterized their device experientially, according to model-based design [10]. Whereas the conductive post array of this device involved the complicated fabrications. Wu et al took advantage of AC-FFET to fixed-potential ICEO mixer, and fabricated the device by integrating the Indium Tin Oxide (ITO) electrode and polydimethylsiloxane (PDMS) channel [9]. Note that the fabrication and expense of the device are very simple and cost-efficient. To simplify the adjustment of signal, Zhang et al developed an efficient micromixer using asymmetrical floating electrodes [8]. Recently, in the experiment, we found the nonuniform electric field generated by asymmetrical driving electrodes can induce ICEO transverse flow over the floating electrode, which is a potential alternative in developing micromixer. To date, no literatures can be found to report such device. These aspects inspirited us to design a micromixer by using ICEO transverse flow actuated by asymmetrical driving electrodes.

In the present work, we demonstrated homogeneous micromixing utilizing ICEO transverse flow actuated by asymmetrical driving electrode sequence. The design of the device is given in Fig.1a and b. Firstly, we conducted the numerical simulations to study the flow field distribution and interface evolution under the ICEO transverse flow, demonstrating the work principle of this method. Secondly, we explored the effects of electrode structure, and electrolyte characteristics on the performance of the micromixers. Thirdly, we fabricated the device and performed the experiment to demonstrate the feasibility of this method. Finally, we experimentally exploited the influences of electric voltage intensity, frequency, and velocity on the capability of the proposed micromixer. The advantages of this mixing method, such as durable performance and flexible adjustment, make it a promising candidate in a wide variety of microfluidic and lab-on-a-chip applications.

2 METHODS AND MATERIALS

2.1 Device design and fabrication

The proposed micromixer mainly consists of PDMS microchannel and glass substrate with ITO electrodes. The Y-shaped PDMS microchannel contains two inlets and an outlet. The fabrication of PDMS microchannel mainly includes three steps: Firstly, the dry film photoresist (RISTON SD238, DUPONT, USS) was processed into designed channel mold through standard soft lithography; Secondly, PDMS (Dow Corning, USA) was cast on the channel mold and baked at 80 ℃ for 2 hours; Thirdly, we peeled PDMS channel off and made holes (inlets and outlet) on the PMDS channel. The fabrication of ITO electrodes includes two steps: Firstly, the desired electrode structure was designed using the software, AutoCAD 2016; Secondly, the transparent ITO film coated on the glass substrate was processed into designed electrode structure through standard soft lithography (AZ4620) and etching (60% of HCl solution and 40% of DI water with Fe_3O_4 powder as catalyst). Moreover, the PDMS channel and glass substrate with ITO electrode was integrated through the bonding technique. The detail fabrication processes can refer to our previous reports [12,13]. The characteristic dimensions of the device are defined in Fig.1 b.

2.2 Experimental setup

In this work, we took advantage of the dilution technique to validate our method and quantitatively evaluate its mixing performance. To characterize the performance of this chip, we injected dyed fluid with fluorescein (Kermel Tianjin) and KCl electrolyte into the channel through two separate inlets. We adjusted conductivity of the dye fluid and KCl electrolyte to 10 μS/cm by adding the DI water. The velocity of two fluids in the microchannel was controlled by a syringe pump (Harvard Apparatus). We observed and recorded the behaviors of two fluids through a fluorescence microscope (IX73, Olympus) with a high-speed CCD camera (Prime 95B). The AC signal
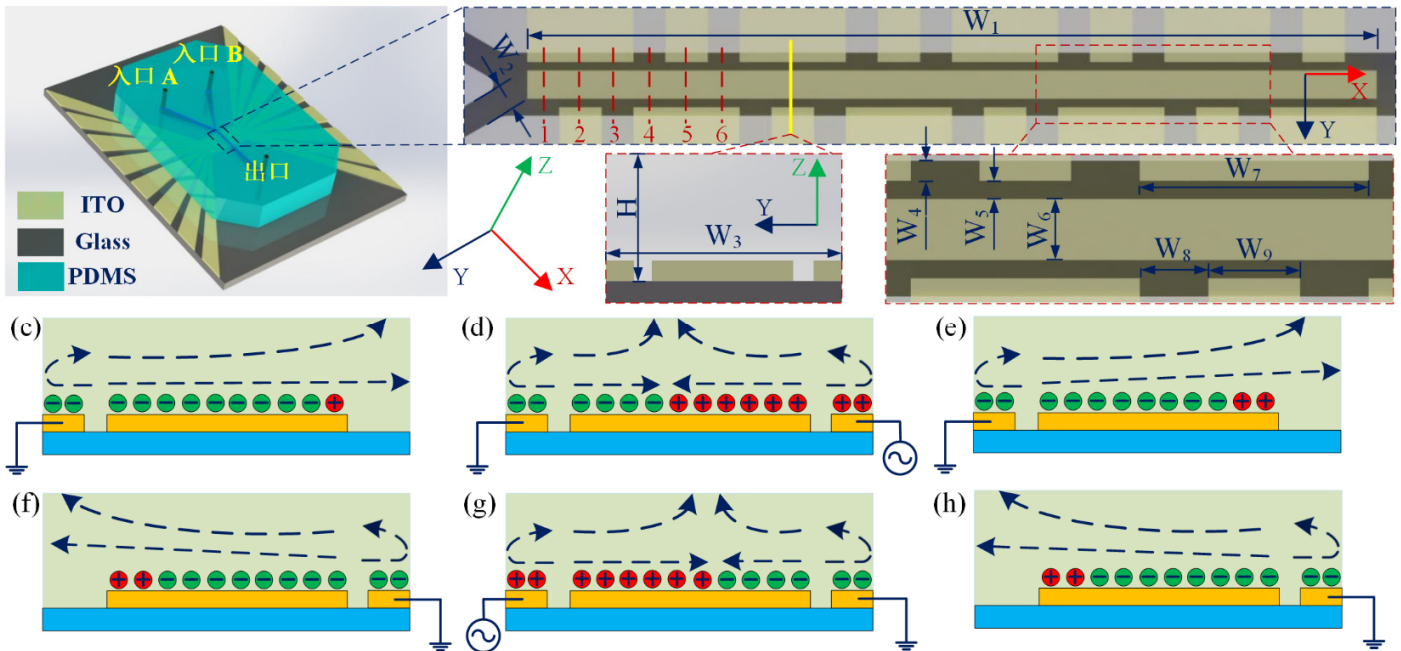
Figure 1: Schematic diagram and principle of micromixer. (a) The 3D diagram of the proposed device. (b) Configuration of the mixing region. (c-e) Mechanism of transverse ICEO flow at the section 1, 2, 3 defined at the first pair of driving electrodes. (f-h) Principle behind the transverse ICEO flow at the section 4, 5, 6 defined at the second pair of driving electrodes.

employed on the asymmetrical driving electrode sequence was generated by a function generator (TGA12104, TTi) and amplified by a signal amplifier (TEGAM). We conducted the numerical simulations by using a FEM software, COMSOL Multiphysics 5.3. The micrographs in the experiment were processed through the software, Image J.

The mixing performance of our micromixer can be quantitatively evaluated according to the following the equation [8]：

$$Me = 1 - \frac{\sqrt{1/n \sum \left(I_i - I_{av}\right)^2}}{I_{av}} \qquad (1)$$

In the simulation, we calculated the mixing efficiency on a Y-Z cross section after passing the floating electrode, where I_i is the concentration of each pixel, n is he number of pixels on the selected section, and I_{av} is average concentration under the ideal mixing. In the experiment, we selected a cutting line after passing the floating electrode to calculate the mixing efficiency, where I_i the fluorescent intensity of each pixel n is he number of pixels on the cutting line, and I_{av} is the average intensity over n pixels.

3 THEORY BACKGROUND

3.1 Principle of ICEO transverse flow

When the voltage signal is employed on the symmetrical driving electrode sequence, the electric field can penetrate the floating electrode surface. With the low frequency ($w < 1/\tau_c$), cations and anions in the solution begin to move along or against the electric field lines [32]. After a characteristic time, $\tau_c = \varepsilon L/\sigma\lambda_D = \lambda_D L/D$, a steady induced double layer (IDL) is established on the interface of bipolar electrode and electrolyte [9]. Under this scenario, IDL screens all the normal electric field and makes the floating electrode turn an ideal insulator. On the one hand, the cations in the diffusive layer close to the positive electrode, under the electric field component parallel to the floating electrode, are pushed toward the centerline of the floating electrode. Meanwhile, the anions in the diffuse layer are dragged to the side of the floating electrode. On the other hand, the cations and anions in the diffusive layer close to the right and left driving electrode have opposite movement direction. Consequently, a pair of counter-rotating ICEO vortices are generated on the floating electrode.

When the driving electrodes become asymmetrical, the ICEO vortices begin to evolve. At the first pair of asymmetrical driving electrode, the narrow driving electrode is employed an AC signal $\phi = A\cos(\omega t)$, while the wide driving electrode is grounded. Under this electric field, at the section 1 and 3, positive charges in the conductor will be accumulated at the top surface of the floating electrode and the negative charges in the solution will be delivered to the interface of electrode and the electrolyte, giving rise to a negatively charge double layer at this interface (Fig.1 c and e). Under the action of the electric field parallel to the Y coordinate on the diffuse layer, transverse ICEO flow from left to right will occur over the floating electrode (Fig.1 b). Meanwhile, at the section 2, a positively charge double layer generated on the floating electrode. Due to larger tangential electric field close to the narrow driving electrode, a pair of

Copyright © 2019 ASME

asymmetrical vortices induce a ICEO flow pointing from right to left side. Contrarily, at the second pair asymmetrical driving electrodes, the distributions of IDL and ICEO flow are opposite to the first pair of driving electrodes, which are presented in Fig.1 f-g, schematically.

3.2 The governing equations

We established a mathematic model to study proposed micromixer by coupling the electric field, flow field, and concentration field. The boundary conditions employed on the model are as follows.

3.2.1 Electric field

Based on the hypothesis that the conductivity of electrolyte is uniform, the electric potential ϕ in the electrolyte can be calculated by solving the Laplace's equation [19].

$$\nabla^2 \phi = 0 \qquad (2)$$

Besides, some boundary conditions should be employed on the microchannel and electrode surface [8]

$$\tilde{\phi} = \tilde{\phi}_0 \qquad \text{at narrow driving electrodes} \qquad (3a)$$
$$\tilde{\phi} = 0 \qquad \text{at wide driving electrodes} \qquad (3b)$$
$$\boldsymbol{n} \cdot \nabla \tilde{\phi} = 0 \qquad \text{at channel wall} \qquad (3c)$$

3.2.2 Flow field

We regarded the fluids needing to be mixed as Newtonian incompressible flow, and the flow field in microchannel is governed by continuity equation and Navier-Stokes equation [22]:

$$\nabla \cdot \vec{u} = 0 \qquad (4)$$

$$\rho \left[\frac{\partial \vec{u}}{\partial t} + \vec{u} \cdot \nabla \vec{u} \right] = -\nabla P + \mu \nabla^2 \vec{u} \qquad (5)$$

where ρ and μ indicate the density and viscosity of the fluid. $\vec{u}$ is the velocity, ∇P is pressure gradient.

By considering the flow in the microchannel as steady flow, we employed the boundary conditions on the channel wall [22]

$$\nabla \cdot P = 0 \qquad \text{in the whole flow field} \qquad (6a)$$
$$\vec{u} = \vec{u}_0 \qquad \text{at the inlet A and B} \qquad (6b)$$
$$P = 0 \qquad \text{at the outlet} \qquad (6c)$$

The tangential electric fields interact with the charges in the diffuse layer on the floating and driving electrodes, which will generate the ICEO and ACEO flow respectively. Therefore, the boundary conditions on the surfaces of floating electrode and driving electrodes should be [30,37]

$$\langle \vec{u}_{ICEO} \rangle = \frac{\varepsilon}{2\eta(1+\delta)} \text{Re}\left(\left(\tilde{\phi} - \frac{\tilde{\phi}_0}{2} \right) \left(\vec{E} - \vec{E} \cdot \vec{n} \cdot \vec{n} \right)^* \right)$$
$$\text{at the floating electrode} \qquad (7a)$$

$$\langle \vec{u}_{ACEO} \rangle = \frac{\varepsilon}{2\eta(1+\delta)} \text{Re}\left(\left(\tilde{\phi} - \tilde{\phi}_0 \right) \left(\vec{E} - \vec{E} \cdot \vec{n} \cdot \vec{n} \right)^* \right)$$
$$\text{at the wide driving electrodes} \qquad (7b)$$

$$\langle \vec{u}_{ACEO} \rangle = \frac{\varepsilon}{2\eta(1+\delta)} \text{Re}\left(\tilde{\phi} \left(\vec{E} - \vec{E} \cdot \vec{n} \cdot \vec{n} \right)^* \right)$$
$$\text{at the right driving electrodes} \qquad (7c)$$

3.2.3 Concentration field

The concentration distribution of the species is governed by [9]

$$\frac{\partial c}{\partial t} + \nabla \left(\vec{u} \cdot c - D\nabla c \right) = 0 \qquad (8)$$

where, the c is the local concentration, D is the diffusion coefficient. Moreover, the boundary conditions on the channel walls are set as [9]:

$$c = 1 \qquad \text{at the inlet A} \qquad (9a)$$
$$c = 0 \qquad \text{at the inlet B} \qquad (9b)$$
$$\vec{n} \cdot D\nabla c = 0 \qquad \text{at the outlet} \qquad (9c)$$
$$\vec{n} \cdot \left(-D\nabla c + \vec{u} \cdot c \right) = 0 \qquad \text{at the other channel walls} \qquad (9d)$$

Numerical simulations illustrating the work principle of the device are presented in Fig.2. The simulation model is given in Fig.2a, which also shows the mixing performance in the microchannel. To further demonstrate the mixing mechanism, we studied the flow and concentration distributions at the Y-Z section 1-6 (Fig.2a). At the section 1, the right vortex at the floating electrode is so weak that the left vortex drives the fluid to move toward right side. As a result, the interface of two fluids is pushed toward right side (Fig.2b). At the section 2, a pair of asymmetrical vortices are produced on the floating electrode, which leads to an ICEO flow pointing from right to left side. Moreover, the vortices have non-ignorable effect on disturbing two fluids. Under this condition, the interface is broken and pushed toward left side. In the section 3, left vortices drive the fluids to move toward right side and mix left fluids. It is noteworthy that the ACEO vortices on the driving electrodes have enhancement effect on the transverse flow and mixing two fluids. After the action of the first pair asymmetrical driving electrodes, the mixing efficiency can reach 52.5%. In the section 4, right vortex generates transverse ICEO flow pointing from right to left side on the floating electrode, which pushes the interface to move toward left side. In the section 5, the left vortices overcome the right vortices and drive the fluids move toward right side. Under this scenario, the interface is pushed toward right side and fluids are mixed by this pair of asymmetrical vortices. In the section 6, the right vortex is dominated to the left one and drives the fluids to move toward left side. Under this circumstance, the fluids are mixed by the strong vortices and interface is pushed toward left side. Therefore, the flow field at the second pair of driving electrodes has opposite distributions to that at the first pair of driving electrodes, which further disturbs the interface and mixes the two fluids, contributing to a mixing efficiency, 73.6%.

We also investigated the transverse velocity of fluid in the channel along the intersections of Y-Z section, 1-6, and a X-Y section with the distance 6 μm to the channel bottom (Figrue.2 h). The fluid flow is no longer symmetrical vortices and becomes
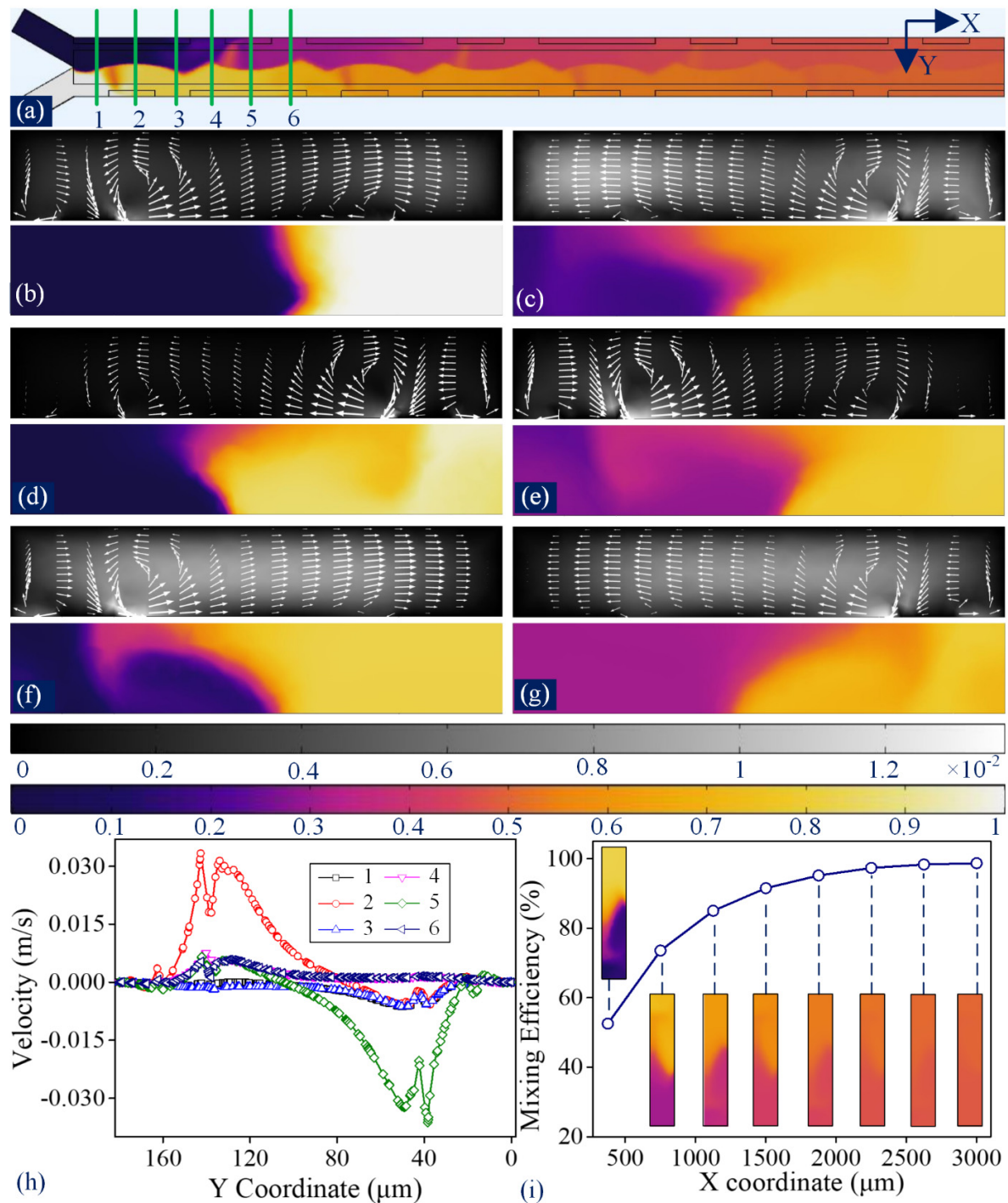
Figure 2: The numerical simulation of the proposed micromixer at u=1500 µm/s, A=10 V, f=200 Hz. (a) Simulation model and concentration distribution in the microchannel. (b-g) The flow field and interface evolution at the Y-Z section 1-6 defined in (a). (h) The transverse flow rate distribution along the Y coordinate. (i) The mixing performance along the X coordinate.

transverse flow. Moreover, the transverse flows around the section 2 and 5 are larger than other locations and play significant roles in the transferring and mixing two fluids. It is noteworthy that the sharp declines of the electric field intensities along section 2 and 5 give rise to the sudden drops of velocities. The contributions of every pair of asymmetrical driving electrodes to the mixing performance are summarized in Fig.2i.
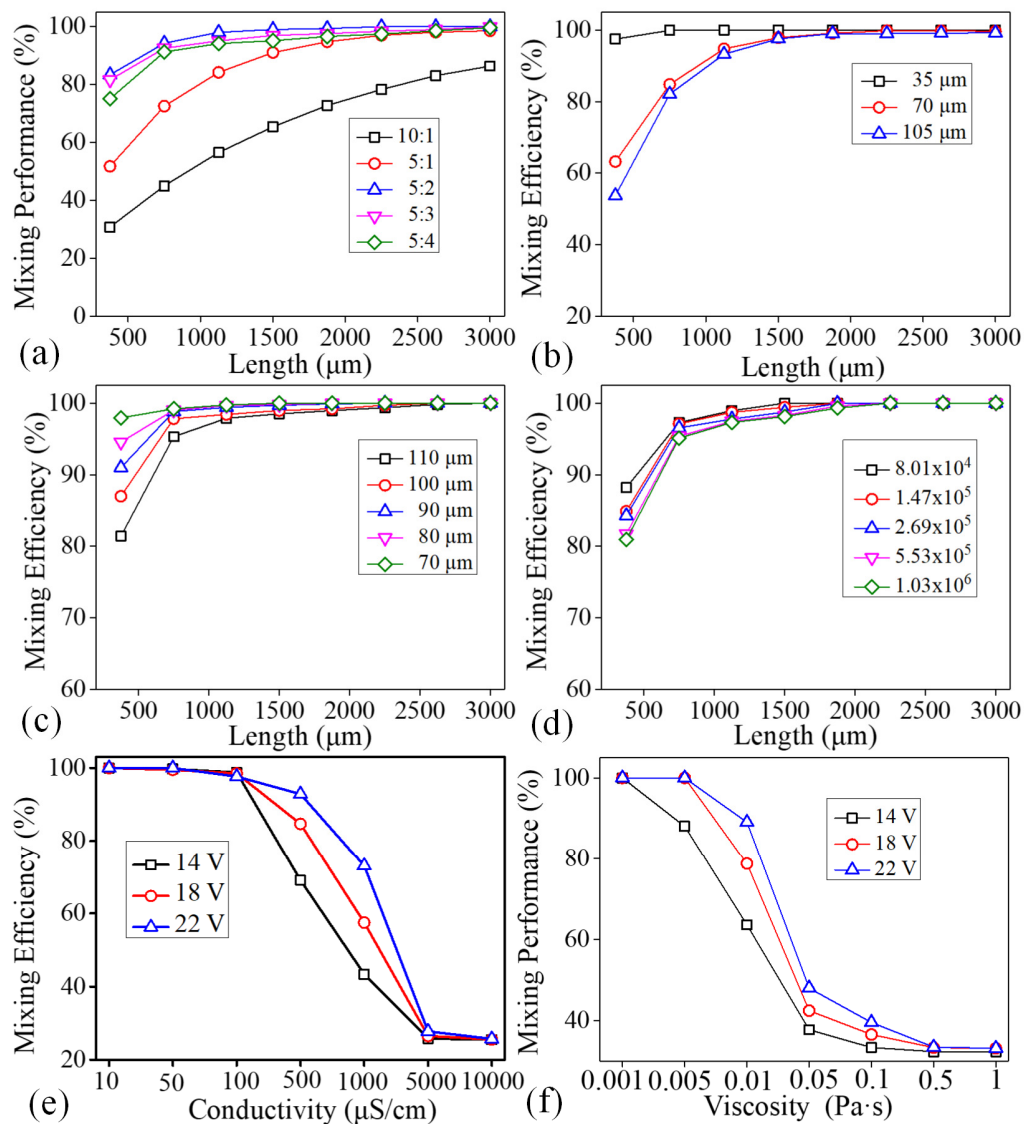
Figure 3: Numerical study of parametric effect on mixing performance at $W_1=3000$ μm, $W_2=80$ μm, $W_4=20$ μm, $W_5=20$ μm and $W_7=375$ μm. (a) The effects of driving electrode width ratio on the mixing capability at $W_3=190$ μm, $W_6=110$ μm, and $H=35$ μm. (b) The effects of channel height on the mixing capability at $W_3=190$ μm, $W_6=110$ μm and $W_7/W_9=5:2$. (c) The effects of floating electrode width on the mixing capability at $H=35$ μm and $W_7/W_9=5:2$. (d) Mesh independency test of the determined simulation model. (e-f) The effects of fluid conductivity and viscosity on the mixing performance.

Table 1. Detail dimensions of the channel and electrode of the micromixer.

Parameter	W_1	W_2	W_3	W_4	W_5	W_6	W_7	W_8	W_9	H
Value (μm)	3000	80	190	20	20	110	375	112.5	150	35

4 RESULTS AND DISCUSSION

4.1 Effects of device structure and electrolyte characteristics on micromixing

To determine reasonable configuration of the device, we firstly explored the influence of the electrode and channel structure on mixing efficiency. The width ratio of the driving electrodes (W_7/W_9) plays an important role in the transverse flow formation. According to Fig.3a, when $W_7/W_9=5:2$, the micromixer has excellent performance. The mechanism behind this phenomenon is that when $W_7/W_9=10:1$ or $5:1$, some areas on the floating electrode will not be covered by the strong tangential electric field, resulting in a weak transverse flow.
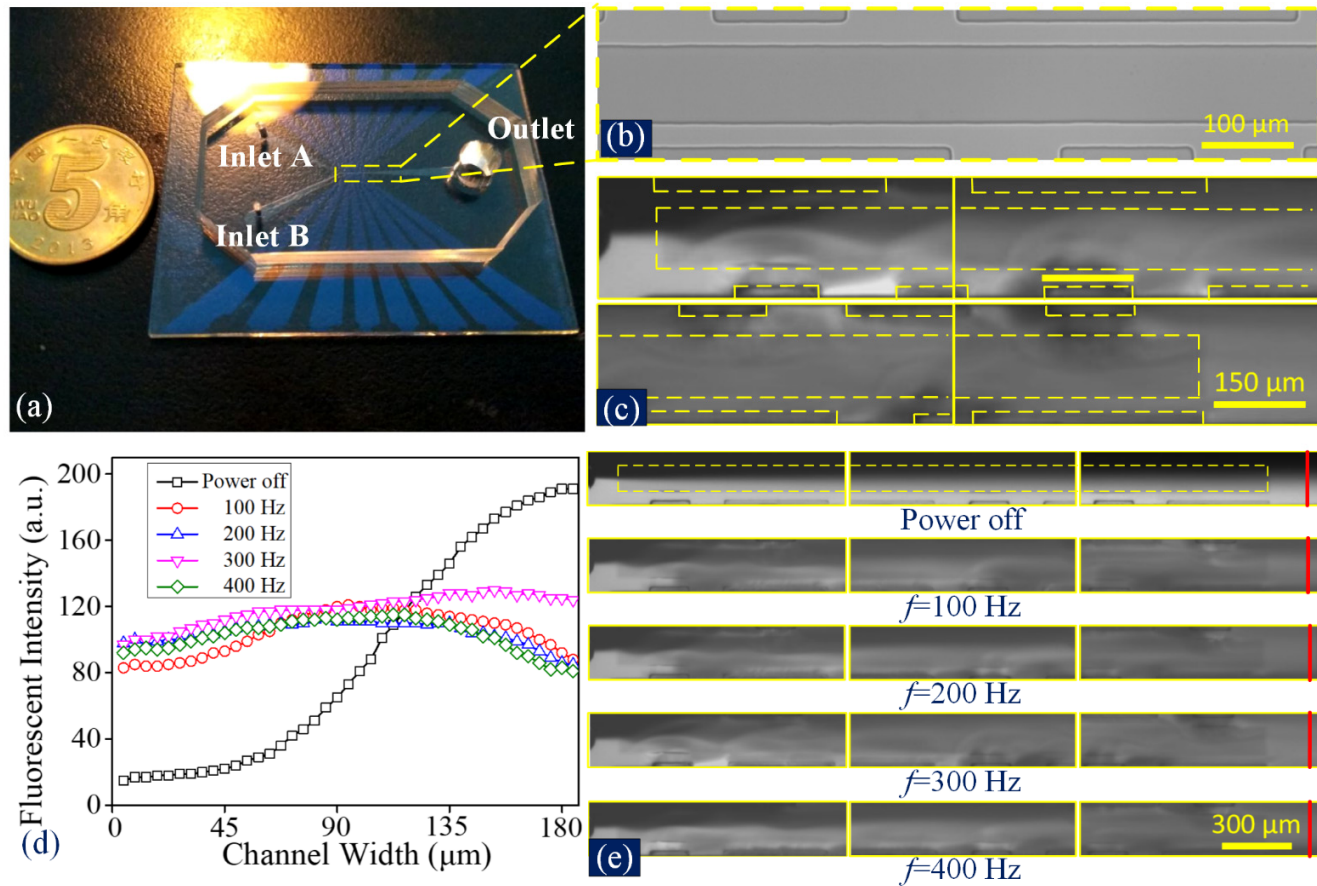
Figure 4: Verification experiment. (a) Actual photograph of the micromixer (b) The micrograph of the channel and electrode configuration. (c) The behaviors of two fluids at the different position of device. (d) Fluorescent intensity distribution along the selected cutting line at power off and under different driving frequencies. (e) Experimental images illustrating the performances of two fluids under the mentioned above conditions.

When W_7/W_9 is increased to 5:3 and 5:4, the electric field trends to be uniform and transverse flow begins to be suppressed. Then, we considered the influence of the channel height, H, on the micromixer performance. Obviously, the device with the channel height of 35 μm has the most excellent performance. One reasonable explanation may be that in the high-channel device, ICEO transverse flow has insufficient strength to drive the fluid near the channel top. We also investigated the effect of floating electrode width, W_6, on the mixing efficiency. As shown in Fig.3c, with decreasing floating electrode width, the micromixer needs a shorter mixing distance at the fixed voltage intensity and frequency. This phenomenon is mainly attributable to that a wider floating electrode needs a higher voltage intensity to produce ICEO transverse flow to cover the whole floating electrode. In term of the mixing performance and throughput, we determined the micromixer configuration: W_7/W_9=5:2, H=35 μm, and W_6=110 μm. We also tested the mesh independency of the determined model by studying tetrahedral grid systems with the element number ranging from 8.01×10^4 to 1.03×10^6. Evidently, when the element number is over 5.53×10^5, the

number of elements has negligible effect on the mixing performance. In the next step, a model with a grid system of 6.68×10^5 elements is selected to conduct further calculation. Depending on the mesh independence of selected model, we explored the effects of electrolyte conductivity and viscosity on the micromixing, which are presented in Fig.3e and f, respectively. As depicted in Fig.3e, with increasing the conductivity from 10 to 100 μS/cm, this chip can obtain acceptable micromixing with the mixing efficiency near 100.0%. With the conductivity over 100 μS/cm, the mixing efficiency begins to decrease drastically. According to Fig.3f, with a driving voltage intensity of 14 V, the mixing efficiency can reach about 100.0% at the viscosity of 0.001 Pa·s, and mixing efficiency will decline to around 30.0% at the viscosity over 0.1 Pa·s. As the voltage intensity increased, the curve demonstrating the dependence of the mixing efficiency on viscosity has no obvious change.

4.2 Verification experiment

After studying this method numerically, we fabricated the experimental setup to validate our method. The actual photograph
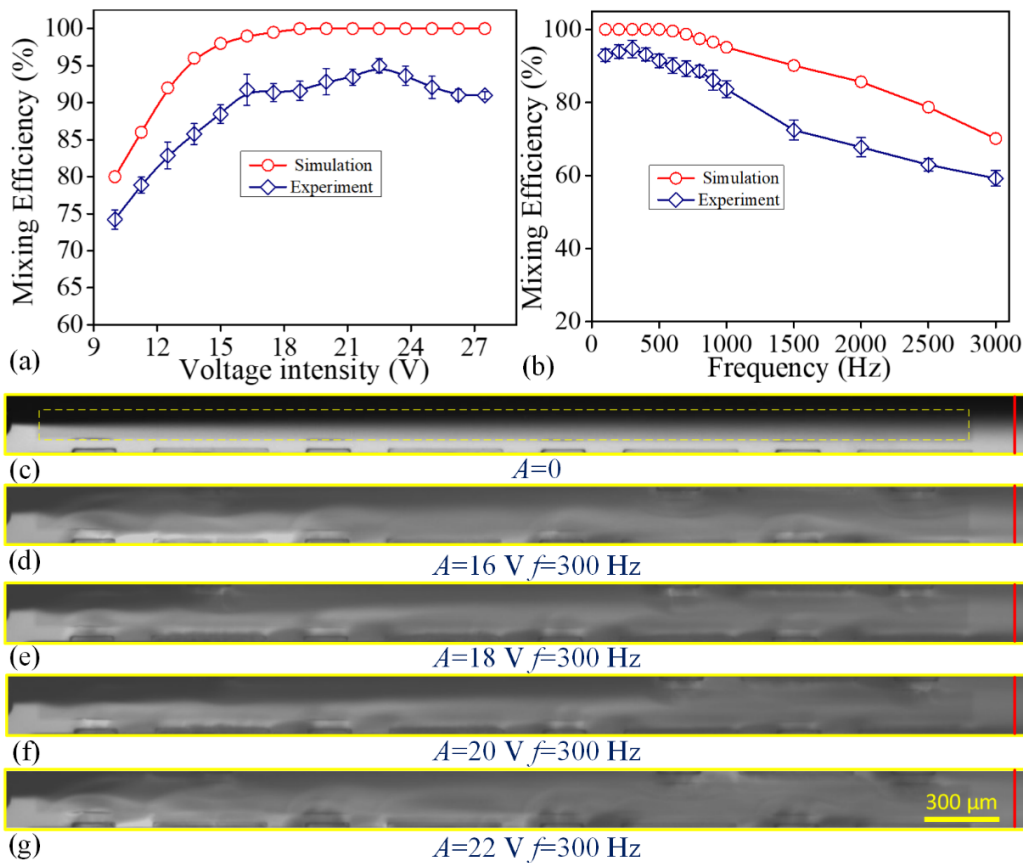
7

Figure 5: Voltage intensity and frequency dependences of mixing efficiency. (a) Plot illustrating the mixing efficiency against voltage (b) Plot demonstrating the mixing efficiency against frequency at A=16, 18, 20.0, and 22 V. (c) Experimental images at different voltage intensities.

of the device is presented in Fig.4a and detail configuration of the channel is given in Fig.4b. The detail dimensions of the channel and electrode of the micromixer in the verification experiment are shown in Table 1. When no AC signal is employed on the driving electrode sequence, two fluids show unmixed laminar flow profile with a clear interface in the microchannel. Upon the actuation of an AC signal, A=20 V, f=100 Hz, the interface of dyed and undyed fluids is disturbed and two fluids are mixed by the cyclic transverse ICEO flow. The mixing behaviors at the different position of device is shown in Fig.4c. With a driving frequency of 200 Hz, the mixing begins to become more acceptable. By increasing the frequency to 300 Hz, we can observe more homogeneous mixing. When the frequency is increased to 400 Hz, the device begins to show uncompleted mixing. To qualitatively characterize the concentration distribution, we measured the fluorescent intensity along selected cutting line, which are summarized in Fig.4d. The corresponding experimental images are presented in Fig.4e.

4.3 Effects of voltage intensity and frequency on micromixing

We explored the influences of the voltage intensity on the mixing performance of the device. The dependence of the mixing capability on the voltage intensity at f= 300 Hz, u=1000 µm/s is

presented in Fig.5a. It is worth noting that with the growth of the voltage intensity, the mixing performance can be enhanced with the voltage intensity from 10 to 16 V. With a driving voltage intensity of A=16 V, the mixing efficiency can reach 92.1%. By increasing the voltage intensity to 18 V, the mixing efficiency exceeds 91.8%. When the voltage intensity is further increased to 20 V, the mixing efficiency exceeds 91.7%. Moreover, the mixing efficiency reach its peak value 94.4% at A=22 V. When the voltage intensity is over 22 V, the mixing efficiency begin to fall. The mechanism behind this phenomenon may be that the strong vortices begin to have obvious focusing effect on fluorescein powder, which makes the distribution of the fluorescein particles don't represent adequately the motion of fluid, reducing the mixing efficiency. According to Fig.5a, despite experimental and numerical results share similar variation trend, the mixing efficiencies in the experiment are below that in the simulation. This phenomenon is caused mainly by the adhesion of the fluorescein powder on the channel walls and focusing of fluorescein powder on the floating electrode [8].

We also studied the dependence of frequency on the mixing capability at A=22 V u=1000 µm/s. According to simulation, we can get homogeneous mixing with the mixing efficiency 100.0% at the frequency ranging from 100 to 500 Hz. With increasing

8

Copyright © 2019 ASME

the frequency over 600 Hz, the mixing efficiency begins to decline slowly. When the frequency is over 1000 Hz, the mixing efficiency decreases sharply. The frequency dependence of mixing efficiency in experiment has similar variation trend to that in simulation, whereas experimental results are below the theoretical prediction. Moreover, the mixing efficiency reaches 94.4% at f=300 Hz. The snapshot illustrating the mixing process at A=0/ A=16 V, f=300 Hz/ A=18 V, f=300 Hz/ A=20 V, f=300 Hz/ A=22 V, f=300 Hz is given in Fig.5c/ d/ e/ f/ g.

4.4 Influence of velocity on micromixing

Furthermore, we investigated the effect of inlet velocity on the mixing performance of the device under different voltage intensities. When the velocity rises from 500 to 4000 μm/s at A=10 V, mixing efficiency reaches its maximum value 74% at u=1000 μm/s and decline sharply to 51.8% at u=4000 μm/s. (Fig.6). When the voltage intensity is increased to 14 V, the mixing efficiency reach the peak value 83.1% at the velocity of 1000 μm/s. By increasing the voltage intensity to 18 and 22 V, the mixing efficiencies obtained their maximum value 91.5% and 94.4%, respectively.
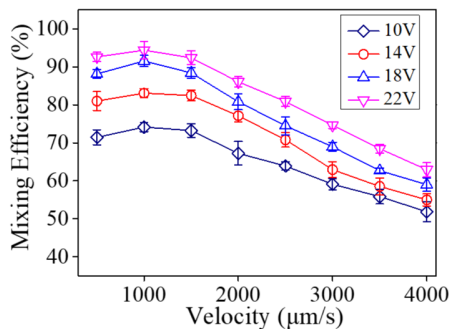

Figure 6: The effect of velocity on the mixing performance at f=300 Hz under different voltage intensities.

CONCLUSION

In this work, we proposed an efficient micromixer based on cyclic ICEO transverse flow. The present device made use of eight pairs of asymmetrical driving electrodes at the bottom of the channel to generate cyclic ICEO transverse flow on the floating electrode. According to the simulations of flow field distribution and interface evolution, strong transverse flow induced by asymmetrical vortices can be formed on the floating electrode. We determined reasonable configuration of the micromixer numerically: W_7/W_9=5:2, W_6=110 μm, and H=35 μm. Depending on the mesh independency test of determined simulation model, we investigated the dependence of the liquid viscosity, and conductivity on the mixing capacity of micromixer. Then, we fabricated the device and conducted the experiment to validate this method. We explored the influences of voltage and frequency on the mixing efficiency and found that the proposed micromixer has an excellent performance with the mixing efficiency 94.4% at A=22 V, f=300 Hz. Furthermore, we studied the effect of the inlet velocity on the capability of the device under different voltage intensities. The advantages of this mixing method, such as durable performance and flexible adjustment, make it a potential alternative in various microfluidic applications, such as analytical chemistry for chemical analysis, bioanalytical chemistry for drug test, microalgae cultivation for biofuel production, and synthetic organic chemistry for nanoparticle synthesis.

ACKNOWLEDGEMENTS

REFERENCES

[1] Garstecki. P. M. J.F., Fischbach, M.A., Sia, S.K., Whitesides, G.M., 2006, "Mixing with bubbles: a practical technology for use with portable microfluidic devices", Lab on a chip, Vol.6, pp207-212, DOI 10.1039/b510843h.

[2] Sasaki, N., Kitamori, T., Kim, H.B., 2006, "AC electroosmotic micromixer for chemical processing in a microchannel", Lab on a chip, Vol.6, pp550-554, DOI 10.1039/b515852d.

[3] Wang, Y., Lin, Q., Mukherjee, T., 2005, "A model for laminar diffusion-based complex electrokinetic passive micromixers", Lab on a chip, Vol.5, pp877-887, DOI 10.1039/b500010f.

[4] Wu, Z., Li, D., 2007, "Mixing and flow regulating by induced-charge electrokinetic flow in a microchannel with a pair of conducting triangle hurdles", Microfluidics and Nanofluidics, Vol.5, pp65-76, DOI 10.1007/s10404-007-0227-7.

[5] Stroock, A.D., Dertinger, S.K.W., Ajdari, A., Igor Mezic, I., Stone, H.A., Whitesides, G.M., 2002, " Chaotic Mixer for Microchannels", Science, Vol.295, pp647-651, DOI DOI: 10.1126/science.1066238.

[6] Hessel, V., Löwe, H., Schönfeld, F., 2005, "Micromixers—a review on passive and active mixing principles", Chemical Engineering Science, Vol.60, pp2479-2501, DOI 10.1016/j.ces.2004.11.033.

[7] Lee, C.Y., Chang, C.L., Wang, Y.N., Fu, L.M., 2011, "Microfluidic mixing: a review", International journal of molecular sciences, Vol.12, pp3263-3287, DOI 10.3390/ijms12053263.

[8] Zhang, K., Ren, Y., Hou, L., Feng, X., Chen, X., Jiang, H., 2018, "An efficient micromixer actuated by induced-charge electroosmosis using asymmetrical floating electrodes" Microfluidics and Nanofluidics, Vol.22 DOI 10.1007/s10404-018-2153-2.

[9] Wu, Y., Ren, Y., Tao, Y., Hou, L., Hu, Q., Jiang, H., 2016, "A novel micromixer based on the alternating current-flow field effect transistor", Lab on a chip, Vol.17, pp186-197, DOI 10.1039/c6lc01346e.

[10] Harnett, C.K., Templeton, J., Dunphy-Guzman, K.A., Senousy, Y.M., Kanouff, M.P., 2008, "Model based design of a microfluidic mixer driven by induced charge electroosmosis", Lab on a chip, Vol.8, pp565-572, DOI 10.1039/b717416k.

Copyright © 2019 ASME

[11] Chen, H., Meiners, J-C., 2004, "Topologic mixing on a microfluidic chip", Applied Physics Letters, Vol.84, pp2193-2195, DOI 10.1063/1.1686895.

[12] Feng, X., Ren, Y., Jiang, H., 2013, "An effective splitting-and-recombination micromixer with self-rotated contact surface for wide Reynolds number range applications", Biomicrofluidics, Vol.7, pp54121, DOI 10.1063/1.4827598.

[13] Feng, X., Ren, Y., Jiang, H., 2014, "Effect of the crossing-structure sequence on mixing performance within three-dimensional micromixers" Biomicrofluidics, Vol.8, pp034106, DOI 10.1063/1.4881275.

[14] Huang, P.H., Xie, Y., Ahmed, D., Rufo, J., Nama, N., Chen, Y., Chan, C.Y., Huang, T.J., 2013 "An acoustofluidic micromixer based on oscillating sidewall sharp-edges", Lab on a chip, Vol.13, pp3847-3852, DOI 10.1039/c3lc50568e.

[15] Kim, S-J., Wang, F., Burns, M.A., Kurabayashi, K., 2009, "Temperature-Programmed Natural Convection for Micromixing and Biochemical Reaction in a Single Microfluidic Chamber", Analytical chemistry, Vol. 81, pp 4510–4516, DOI 10.1021/ac900512x.

[16] Ng, W.Y., Goh, S., Lam, Y.C., Yang, C., Rodriguez, I., 2009. "DC-biased AC-electroosmotic and AC-electrothermal flow mixing in microchannels", Lab on a chip, Vol.9, pp802-809, DOI 10.1039/b813639d.

[17] Wen, C.Y., Yeh, C.P., Tsai, C.H., Fu, L.M., 2009, "Rapid magnetic microfluidic mixer utilizing AC electromagnetic field", Electrophoresis, Vol.30, pp4179-4186, DOI 10.1002/elps.200900400.

[18] Ryu, K.S., Shaikh, K., Goluch, E., Fan, Z., Liu, C., 2004, "Micro magnetic stir-bar mixer integrated with parylene microfluidic channels", Lab on a chip, Vol.4, pp608-613, DOI 10.1039/b403305a.

[19] Wu, Z., Li, D., 2008, "Micromixing using induced-charge electrokinetic flow", Electrochimica Acta, Vol.53, pp5827-5835, DOI 10.1016/j.electacta.2008.03.039.

[20] Huang, S-H., Wang, S-K., Khoo, H.S., Tseng, F-G., 2007, "AC electroosmotic generated in-plane microvortices for stationary or continuous fluid mixing", Sensors and Actuators B: Chemical, Vol.125, pp326-336, DOI 10.1016/j.snb.2007.01.046.

[21] Sasaki, N., Kitamori, T., Kim, H.B., 2012, "Fluid mixing using AC electrothermal flow on meandering electrodes in a microchannel", Electrophoresis, Vol.33, pp2668-2673, DOI 10.1002/elps.201200099.

[22] Daghighi, Y., Li, D., 2013 "Numerical study of a novel induced-charge electrokinetic micro-mixer", Analytica chimica acta, Vol.763, pp28-37, DOI 10.1016/j.aca.2012.12.010.

[23] Zhang, K., Mi, X-J., Yu, M-Z., 2012, "Design of super-efficient mixer based on induced charge electroosmotic", Thermal Science, Vol.16, pp1534-1538, DOI 10.2298/tsci1205534z.

[24] Davidson, S.M., Andersen, M.B., Mani, A., 2014, "Chaotic induced-charge electro-osmosis", Physical review letters, Vol.112, pp128302, DOI 10.1103/PhysRevLett.112.128302.

[25] Jain, M., Yeung, A., Nandakumar, K., 2009, "Induced charge electro osmotic mixer: Obstacle shape optimization", Biomicrofluidics, Vol.3, pp22413, DOI 10.1063/1.3167279.

[26] Jia, Y., Ren, Y., Jiang, H., 2015, "Continuous-flow focusing of microparticles using induced-charge electroosmosis in a microfluidic device with 3D AgPDMS electrodes", RSC Advances, Vol.5, pp66602-66610, DOI 10.1039/c5ra14854e.

[27] Ren, Y., Liu, J., Liu, W., Lang, Q., Tao, Y., Hu, Q., Hou, L., Jiang, H., 2016, "Scaled particle focusing in a microfluidic device with asymmetric electrodes utilizing induced-charge electroosmosis", Lab on a chip, Vol.16, pp2803-2812, DOI 10.1039/c6lc00485g.

[28] Ren, Y., Liu, W., Jia, Y., Tao, Y., Shao, J., Ding, Y., Jiang, H., 2015, "Induced-charge electroosmotic trapping of particles", Lab on a chip, Vol.15, pp2181-2191, DOI 10.1039/c5lc00058k.

[29] Liu, W., Shao, J., Ren, Y., Liu, J., Tao, Y., Jiang, H., Ding, Y., 2016, "On utilizing alternating current-flow field effect transistor for flexibly manipulating particles in microfluidics and nanofluidics", Biomicrofluidics, Vol.10, pp034105, DOI 10.1063/1.4949771.

[30] Chen, X., Ren, Y., Liu, W., Feng, X., Jia, Y., Tao, Y., Jiang, H., 2017, "A Simplified Microfluidic Device for Particle Separation with Two Consecutive Steps: Induced Charge Electro-osmotic Prefocusing and Dielectrophoretic Separation", Analytical chemistry, Vol.89, pp9583-9592, DOI 10.1021/acs.analchem.7b02892.

[31] Wu, Y., Ren, Y., Tao, Y., Hou, L., Jiang, H., 2016, "Large-Scale Single Particle and Cell Trapping based on Rotating Electric Field Induced-Charge Electroosmosis", Analytical chemistry, Vol.88, pp11791-11798, DOI 10.1021/acs.analchem.6b03413.

[32] Squires, T.M., Bazant, M.Z., 2004, "Induced-charge electro-osmosis", Journal of Fluid Mechanics, Vol.509, pp217-252, DOI 10.1017/s0022112004009309.

[33] Jain, M., Yeung, A., Nandakumar, K., "Efficient micromixing using induced-charge electroosmosis", Journal of microelectromechanical systems, Vol.18, pp376-384, DOI 10.1109/JMEMS.2008.2010849

[34] Alipanah, M., Ramiar, A., 2017, "High efficiency micromixing technique using periodic induced charge electroosmotic flow: A numerical study", Colloids and Surfaces A: Physicochemical and Engineering Aspects, Vol.524, pp53-65, DOI 10.1016/j.colsurfa.2017.04.020.

[35] Qian, S., Bau, H., 2002, "A Chaotic Electroosmotic Stirrer", Analytical chemistry, Vol.74, pp 3616-3625, DOI 10.1021/ac025601i.

[36] Zhao, H., Bau, H.H., 2007, "Microfluidic chaotic stirrer utilizing induced-charge electro-osmosis", Physical review E, Statistical, nonlinear, and soft matter physics, Vol.75, pp066217, DOI 10.1103/PhysRevE.75.066217.

[37] Chen, X., Ren, Y., Hou, L., Feng, X., Jiang, T., and Jiang, H., 2019, "Induced charge electro-osmotic particle separation", Nanoscale, DOI 10.1039/C8NR09148J.